2016

Behavior of R410A Low GWP Alternative Refrigerants DR-55, DR-5A, and R32 in the Components of a 4-RT RTU

Kenneth Schultz

Trane Technologies, United States of America, kschultz@tranetechnologies.com

Behavior of R410A Low GWP Alternative Refrigerants DR-55, DR-5A, and R32 in the Components of a 4-RT RTU

Kenneth SCHULTZ

Ingersoll Rand
La Crosse, WI, USA
608-787-3735, kschultz@irco.com

ABSTRACT

Concerns about the impact on the environment of the refrigerants used in HVAC&R equipment are driving the development of alternative refrigerants with lower global warming potentials (GWPs). This paper reports the performance of DR-55 (now designated as R452B), DR-5A (now designated as R454B), and R32 in comparison to R410A at the component level from tests run on a 4 RT (14 kW) commercial unitary rooftop heat pump. Overall unit performance was previously reported (Schultz and Kujak, 2016), showing DR-55 and DR-5A to be design-compatible replacement candidates for R410A. This paper further confirms this by comparing performance at the compressor, evaporator, and condenser component level.

1. INTRODUCTION

Concerns about the climate impacts of refrigerants used in HVAC&R equipment are driving development and evaluation of alternative refrigerants with lower global warming potentials (GWPs) to replace R410A. The Air Conditioning, Heating, and Refrigeration Institute (AHRI) began coordinating the Low-GWP Alternative Refrigerants Evaluation Program (AREP) in 2011. Phase II of AREP was recently completed in which new and more optimized refrigerant candidates were proposed and tested. Reports by the participants are available at AHRI (2016).

R32 has received significant attention as a potential replacement for R410A. Indeed, products employing R32 have been announced and are now commercially available. However, R32's flammability limits refrigerant charge sizes allowed by current standards and codes. In addition, R32 has a higher specific capacity (7% to 8%) than R410A, necessitating a re-matching of compressor displacements and heat exchanger capacities. Blends of R32 with R1234yf can offer specific capacities closer to R410A while also having lower GWPs and lower burning velocities. In this regard, the blend labeled DR-5A (R454B) was selected for further evaluation here (Hughes and Leck, 2015).

It is recognized that the flammability (eg, burning velocity) of refrigerant blends can be reduced by the use of R125. Kujak and Schultz (2015, 2016) described a blend labeled DR-55 (now designated as R452B) that balances flammability, performance, and GWP. The thermodynamic properties of DR-55 indicate capacities within a few percent of R410A while offering ~1% higher efficiency. DR-55's burning velocity (~3 cm/s for the nominal composition) is lower than R32's (6.7 cm/s) while matching R32's GWP (675). DR-55 was selected for further study here because of its prospects for being a design compatible alternative to R410A.

The performance of a 4 RT (14 kW), 11 EER (3.22 COP) commercial unitary rooftop heat pump was measured with R410A as a baseline and with the alternative refrigerants DR-55, DR-5A, and R32. DR-55 and DR-5A were observed to have performance characteristics very similar to R410A as predicted a thermodynamic cycle model. R32 required the largest adjustment in compressor speed to match R410A capacity and produced significantly higher compressor discharge temperatures, consistent with the thermodynamic cycle model. Overall unit performance is described by Schultz and Kujak (2016). Additional information can be found in Schultz, et al (2015a,b).

2. REFRIGERANT CHARACTERISTICS

The compositions and GWPs of the refrigerants considered here are listed in Table 1. Select thermodynamic properties are listed in Table 2. The alternatives have slightly higher critical temperatures and have wider saturation domes than R410A. This should allow the alternatives to perform somewhat better at higher ambient temperatures.

Table 1. Compositions and GWPs of the Refrigerants Considered Here.

Refrig	%wt R32	%wt R125	%wt R1234yf	GWP_{AR4}	GWP_{AR5}
R410A	50	50	–	2088	1924
DR-55 / R452B	67	7	26	698	675
DR-5A / R454B	68.9	–	31.1	466	466
R32	100	–	–	675	677

Table 2. Thermodynamic Properties of the Refrigerants Considered Here.

Refrig	Tcritical °F / °C	Pcritical psia / MPa	hfg @ 77°F/25°C Btu/lbm / kJ/kg	CAP*	COP*	CDT °F / °C	glide °Fd / °Cd
R410A	160.4 / 71.3	711 / 4.90	80.20 / 186.6	0	0	171 / 77	0.2 / 0.1
DR-55	175.4 / 79.7	803 / 5.53	94.19 / 219.1	–0.027	+0.012	180 / 82	2.2 / 1.2
DR-5A	177.7 / 80.9	814 / 5.61	95.93 / 223.1	–0.036	+0.013	180 / 82	2.6 / 1.4
R32	172.6 / 78.1	839 / 5.78	116.55 / 271.1	+0.076	+0.010	198 / 92	0 / 0

CAP*, COP*, CDT, and glide are based on a simple thermodynamic cycle operating between an average condensing temperature of 115°F/46.1°C with 15°Fd/8.3°Cd of subcooling and an average evaporating temperature of 53°F/11.7°C with 15°Fd/8.3°Cd of compressor suction superheat. These conditions were typical of the RTU running at the AHRI Standard 210/240 "A" rating conditions (95°F/35°C outdoor temperature). The isentropic efficiency of the compressor is taken as 0.7.

In this work, refrigerant properties are based on REFPROP v9.1 (Lemmon, et al, 2013) with the R32/R1234yf and R125/R1234yf interaction parameters provided by Chemours (formerly DuPont) (Minor, 2012).

3. EQUIPMENT USED

A standard production rooftop heat pump was used for these tests. The unit is rated at a net cooling capacity of 48,500 Btu/hr (4.04 RT, 14.2 kW) at a SEER of 13.0 Btu/W·hr (SCOPc of 3.81). The unit was driven by a fixed speed scroll compressor lubricated with Emkarate RL32H POE oil. The indoor and outdoor heat exchangers were of aluminum-fin/copper-tube construction with fixed speed fans. Adjustable TXVs were installed to allow matching of compressor suction superheats. An adjustable frequency drive (AFD) was installed to allow the compressor speed to be varied so that all refrigerants could be tested at the same capacity, thereby matching compressor capacity to heat exchanger capacity. Measurement of compressor input power was made upstream of the AFD, with efficiency essentially constant over the range of power and speeds tested and assumed to be the cataloged value of 0.97.

Pressure transducers were installed on the refrigerant-side upstream and downstream of key components, providing the ability to measure pressure drops through refrigerant lines as well as through the heat exchangers and the pressure rise across the compressor. Calibrated thermocouples were attached to the refrigerant piping at coincident locations. Additional thermocouples were attached to each end of each circuit of both the indoor and outdoor heat exchangers. Turbine flow meters were installed between each heat exchanger and the corresponding expansion valve to measure the refrigerant flow rate in both cooling and heating modes. Refrigerant mass flow rate is determined from the measured volume flow rate multiplied by the liquid density computed from the temperature measured just upstream of the flow meter, $\dot{m}_{refrig} = \dot{V}_{r,meter}\rho(T_{meter})$.

4. DESCRIPTION OF TESTS

Tests were conducted in a pair of controlled ambient chambers. The method of test was consistent with Appendix M of AHRI Standard 210/240 (2008/2012), with operating conditions generally held within tighter tolerances.

Tests were first run with R410A to establish the baseline performance of the unit. Refrigerant charge was determined while operating at the AHRI "A" conditions, 80°F dry bulb/67°F wet bulb (26.7°C/19.4°C) indoor and 95°F (35°C) outdoor. For each subsequent refrigerant, a charge sweep was also run at the "A" conditions. The charge was selected to maximize unit efficiency (EER/COP). The TXV was also adjusted during the early runs to deliver the target compressor suction superheat obtained with R410A (~13°Fd/7°Cd). Runs were then made to determine the compressor speed that produced a match to R410A capacity at the "A" rating conditions to within ±1%; this speed was then used for all subsequent tests with that refrigerant. A series of tests was then executed at the rating points called out in AHRI Standard 210/240. In addition, tests were also run with the outdoor temperature varying from 65°F to 125°F (18°C to 52°C) to examine performance over a wide range of ambient temperatures.

5. SYSTEM ENERGY BALANCE

The comparison of cooling capacities measured on the air-side and refrigerant-side (indoor coil as evaporator) as outdoor/ambient temperature is varied is shown in Figure 1. The results indicate there is heat transfer between the indoor air stream and the surrounding ambient. This heat transfer "loss" should be independent of the refrigerant being used (no horizontal shift). The differences, then, could be attributable to small biases in refrigerant properties (possibly liquid density; see below). Trusting the R410A properties suggests that ~65% of the heat loss occurs from the return air stream and ~35% from the delivered air stream. Figure 2 shows the heat loss plotted against the difference between the ambient temperature and the weighted average of the indoor air stream temperatures. Making small (vertical) adjustments (the A_i's referenced below) to the computed refrigerant-side heat transfer rates results in very similar heat transfer losses for all refrigerants tested. The slopes of the lines indicate the heat loss conductance (UA) of the indoor air duct is between 80-100 Btu/hr·°Fd (41-53 W/°Cd).

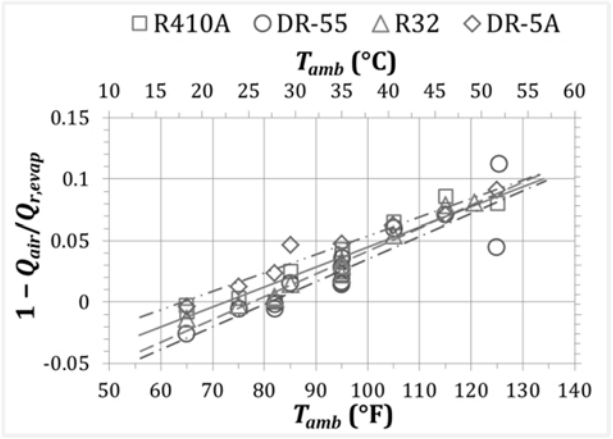

Figure 1. Heat transfer "loss" from the indoor air stream to the surroundings as a function of ambient temperature.

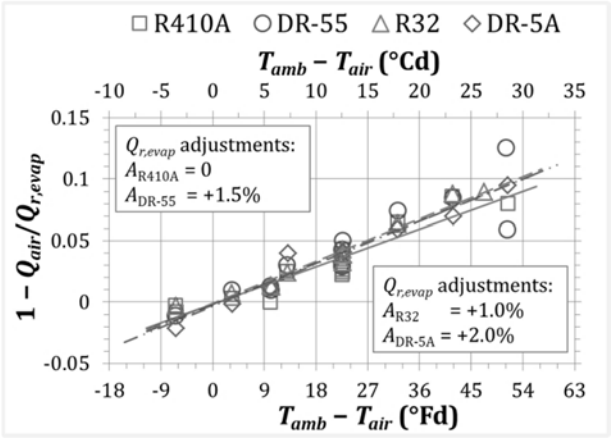

Figure 2. Adjusted heat transfer "loss" from the indoor air stream to the surroundings as a function of the difference between the ambient temperature and the weighted average indoor air temperature.

6. COMPRESSOR PERFORMANCE

The volumetric flow rate of the refrigerant entering the compressor suction can be computed from the measured refrigerant mass flow rate multiplied by the specific volume determined from the measured suction temperature and pressure. Dividing this by the volumetric displacement of the compressor times the rotational speed gives a representative volumetric efficiency,

$$\eta_{vol} = \dot{V}_{r,suc}/\left(V_{cmpr}S_{cmpr}\right) = \left((1 - A_i)\dot{m}_{refrig}\upsilon(T_{suc}, P_{suc})\right)/\left(V_{cmpr}S_{cmpr}\right) \quad (1)$$

The volumetric efficiencies obtained during cooling operation are shown in Figure 3, plotted against the compressor discharge to suction pressure ratio. Here, the adjustments (A_i's) made above (see Figure 2) to the refrigerant-side heat

transfer rates to collapse the energy balance lines are applied to the refrigerant liquid densities[1] (assuming that the turbine meter response is independent of the fluid). This brings the volumetric efficiencies with DR-55 and DR-5A within ~one percentage point of R410A (η_{vol} runs 0.02 to 0.03 below R410A without the adjustments). The volumetric efficiency with R32 ranges from 0.02 below R410A to 0.04 below as pressure ratio increases (0.035 to 0.05 below without the adjustments). The decreases in volumetric efficiencies from R410A to DR-55 and DR-5A down to R32 correspond to increases in suction specific volumes from R410A (0.40 ft³/lbm / 0.025 m³/kg at 95°F / 35°C ambient temperature) to DR-55 and DR-5A (0.48 ft³/lbm / 0.030 m³/kg) to R32 (0.55 ft³/lbm / 0.034 m³/kg).

An isentropic efficiency can be computed by dividing the isentropic enthalpy rise from the suction condition to the discharge pressure by the measured compressor power input divided by the measured refrigerant mass flow rate,

$$\eta_{isen} = \left(h(s_{suc}, P_{dis}) - h(T_{suc}, P_{suc})\right) / \left(\dot{W}_{cmpr} / \left((1 - A_i)\dot{m}_{refrig}\right)\right) \quad \text{where} \quad s_{suc} = s(T_{suc}, P_{suc}) \tag{2}$$

The isentropic efficiencies during cooling operation are shown in Figure 4. Isentropic efficiencies are observed to peak near the "A" rating condition, falling off on either side. Using the refrigerant flow rate adjustments noted above collapses the efficiencies for all refrigerants, except for R32 at higher ambient temperatures, possibly related to R32's significantly higher discharge temperatures. This is consistent with the increase in compressor power consumed by R32 relative to the other refrigerants as ambient temperature increased above 95°F/35°C (Schultz and Kujak, 2016; Schultz, et al, 2015a).

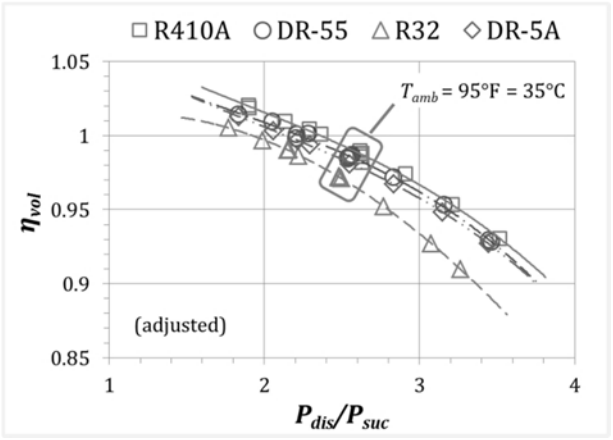

Figure 3. Compressor volumetric efficiencies by Eq (1) using the adjustment parameters listed in Figure 2.

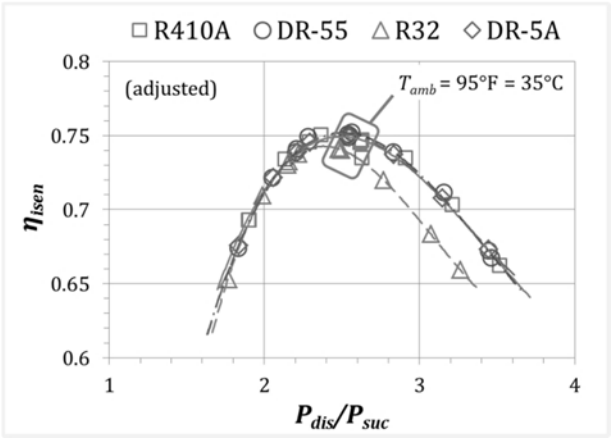

Figure 4. Compressor isentropic efficiencies by Eq (2) using the adjustment parameters listed in Figure 2.

An energy balance around the compressor indicates that not all of the power input to the compressor gets transferred to the main refrigerant stream. The energy lost from the compressor is computed as the difference between the power input to the compressor and the difference between the measured discharge and suction enthalpies multiplied by the (adjusted) refrigerant mass flow rate, $\dot{Q}_{cmpr,l} = (1 + A_i)\dot{m}_{refrig}\left(h(T_{dis}, P_{dis}) - h(T_{suc}, P_{suc})\right)/\dot{W}_{cmpr}$, is very similar for all refrigerants, being 10% to 11% of the power input at T_{amb} = 95°F/35°C, increasing to ~12% at lower and higher ambient temperatures. The loss with R32 increases to ~13% as ambient temperature increases toward the 120°F/49°C maximum outdoor temperature achieved where the compressor discharge temperature safety limit was reached.

7. INDOOR COIL AS EVAPORATOR

The indoor coil consists of eight parallel circuits. Pressures and temperatures were measured upstream of the distributor and downstream of the collection point. Temperatures were also recorded from thermocouples attached to the entrance and exit of each circuit. The temperatures reported at the circuit entrances were uniform with standard deviations generally between 0.3°Fd and 0.8°Fd (0.15°Cd and 0.45°Cd). Assuming a saturated condition at the

[1] Note that REFPROP lists the uncertainty in liquid density as 0.05% for R32 and 0.1% for R125 and R1234yf.

entrance of each circuit indicates that a large portion of the overall pressure drop occurs across the distributor. The pressure drop across the evaporator will be taken here as the difference between the saturation pressure calculated from the average coil entrance temperature and the pressure measured downstream of the collection point.

The amount of superheat generated by the evaporator was quite small here, generally less than 2°Fd/1.1°Cd; the majority of the pressure drop therefore is due to two-phase fluid flow. (The compressor suction superheat comes mainly from heat transfer across the four-way cooling/heating mode switching valve.) The evaporator pressure drops are plotted against refrigerant mass flow rate in Figure 5. The larger symbols represent tests run with a fixed indoor return air condition while varying the ambient outdoor temperature. The smaller symbols represent tests run with a fixed outdoor temperature while varying the indoor return air condition. The pressure drop obeys a power law model with an exponent of approximately 1.6. Note the progression from highest flow rate with R410A (narrowest dome) to lowest flow rate with R32 (widest dome).

Figure 6 shows the change in saturation temperature from the coil circuit entrance (as measured) to the common mixed outlet (dew point associated with the measured pressure). With R410A, the heat exchanger pressure drop created a "negative temperature glide" of ~4°Fd/2.2°Cd. Because of its lower mass flow rate and pressure drop, R32 experienced a smaller temperature glide of ~2°Fd/1.1°Cd. Although DR-55 has a pressure drop intermediate to R410A and R32, its effective temperature glide is reduced to ~1.5°Fd/0.8°Cd by DR-55's inherent thermodynamic temperature glide of ~2.0°Fd/1.1°Cd. The effective temperature glide is even smaller for DR-5A because its slightly larger thermodynamic glide of 2.4°Fd/1.3°Cd further offsets the negative glide from the pressure drop.

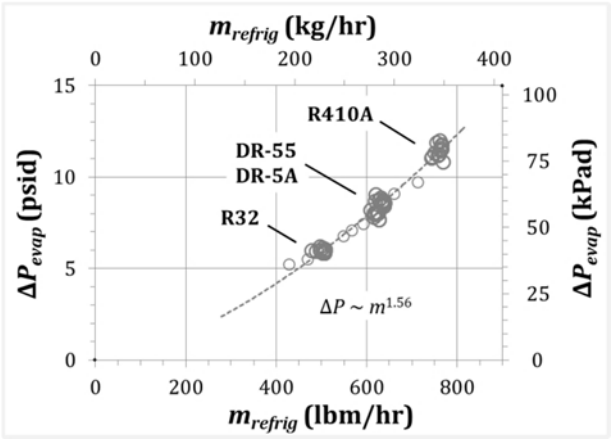

Figure 5. Pressure drop across the indoor coil (evaporator) as a function of refrigerant mass flow rate.

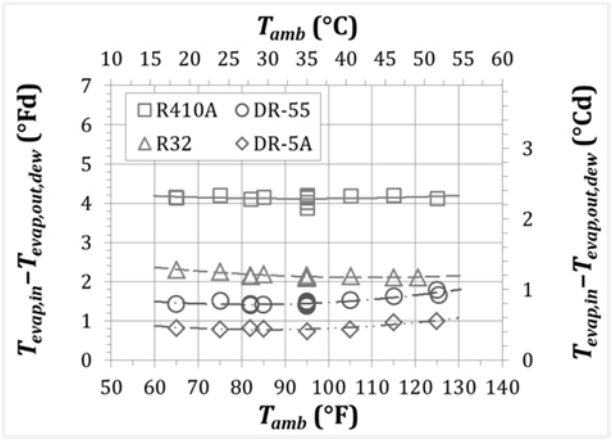

Figure 6. Change in saturation temperature across the evaporator, ie, the effective (negative) glide.

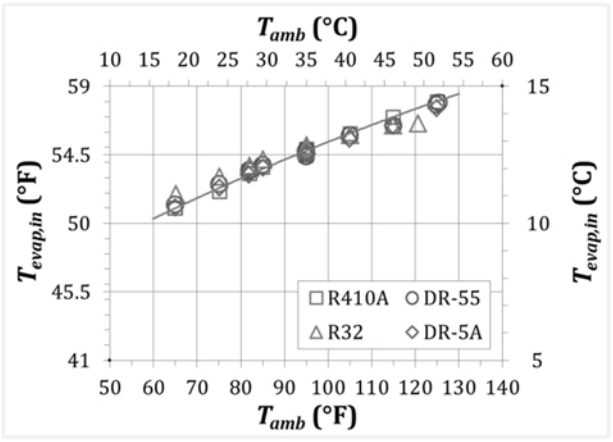

Figure 7. Averages of the measured temperatures entering indoor (evaporator) coil circuits.

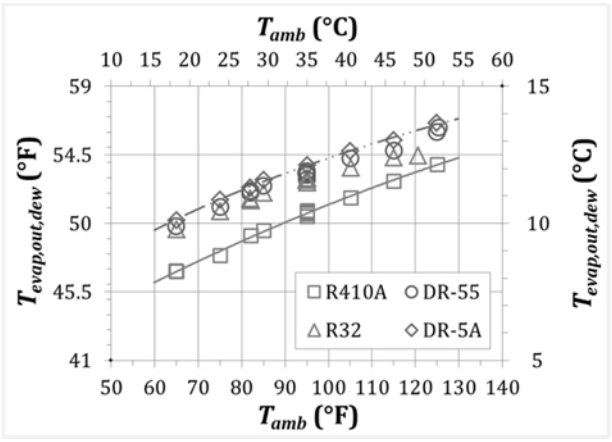

Figure 8. Dew point temperatures leaving the indoor (evaporator) coil (downstream of collection point).

Figure 7 shows that the evaporator entering temperatures were nearly the same for all four refrigerants. The corresponding exit dew points are shown in Figure 8 (Figure 6 subtracted from Figure 7). The higher exit dew points for DR-55 and DR-5A, and even R32, result in relatively higher compressor suction pressures and lower lifts compared to R410A. A simple thermodynamic cycle model assuming fixed compressor displacement and matching average saturation temperatures in the evaporator indicates that DR-55 should fall short of R410A's capacity by ~2.5% at the "A" conditions and offer a ~1% increase in efficiency (see Table 2). The ~2.5°Fd/1.4°Cd increase in evaporator exit dew point and consequently higher suction vapor density with DR-55 offsets its thermodynamic shortfall in capacity, providing a match to R410A capacity without having to change compressor displacement or speed. The ~2.5°Fd/1.4°Cd increase in evaporator exit dew point and consequently lower lift with DR-55 also adds ~5% to its efficiency advantage over R410A.

8. OUTDOOR COIL AS CONDENSER

The outdoor coil also consists of eight parallel circuits. Pressures and temperatures were measured upstream and downstream of the condenser. Temperatures were also recorded from thermocouples attached to the entrance and exit of each circuit. The temperatures reported at the circuit entrances generally varied less than ±3.5°Fd/±2°Cd with a consistent pattern independent of operating condition and refrigerant. The circuit exit temperatures showed a general trend of being warmer leaving the top circuit to colder leaving the bottom circuit, likely due to non-uniform air flow across the coil face; the pattern was independent of refrigerant.

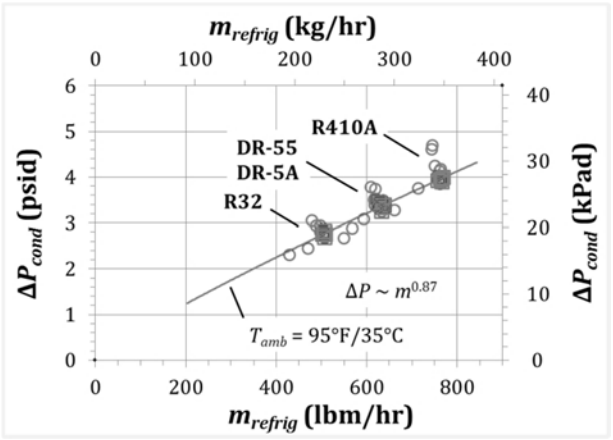

Figure 9. Pressure drop across the outdoor coil (condenser) as a function of refrigerant mass flow rate.

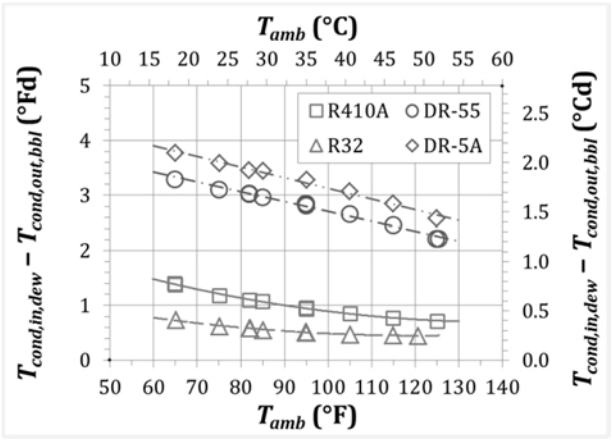

Figure 10. Change in saturation temperature across the outdoor coil (condenser).

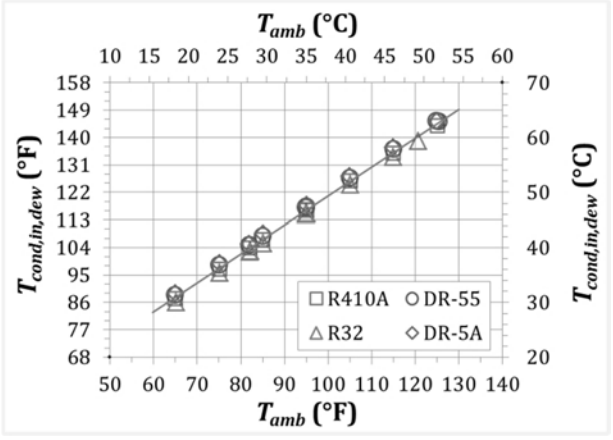

Figure 11. Refrigerant dew point temperatures entering the outdoor coil (condenser).

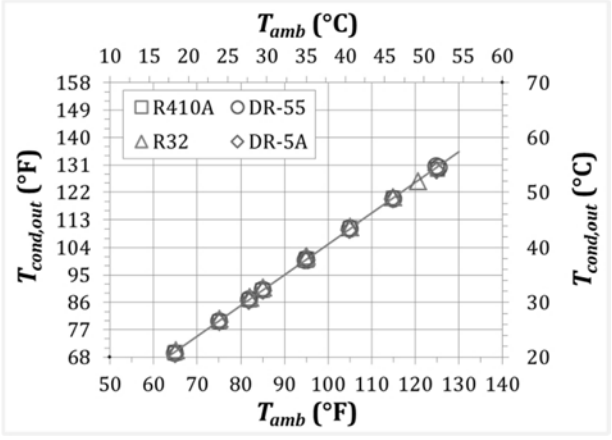

Figure 12. Refrigerant temperatures exiting the outdoor coil (condenser).

The overall pressure drop across the condenser as a function of refrigerant mass flow rate is shown in Figure 9. The condenser pressure drop is less sensitive to mass flow rate than is the evaporator, having a power law exponent of ~0.9. The condenser pressure drops are approximately one-third (R410A) to one-half (R32) of the evaporator pressure drops. The corresponding differences between entrance and exit saturation temperatures are shown in Figure 10. At T_{amb} of 95°F/35°C, the ~4 psid/28 kPad pressure drop experienced by R410A translates into a 1°Fd/0.6°Cd drop in saturation temperature. The effective temperature glide with R32 is roughly half of R410A's. On the other hand, the inherent thermodynamic temperature glide of DR-55 and DR-5A adds to the glide from the pressure drop, resulting in effective temperature glides of ~3°Fd/1.7°Cd at T_{amb} of 95°F/35°C.

As explained in Schultz and Kujak (2016) and Schultz, et al (2016a), the refrigerant charge for each refrigerant was selected to maximize the unit efficiency at the "A" conditions. This resulted in slightly different subcoolings at the condenser exit ranging from 13.5°Fd/7.5°Cd for R32 up to 15°Fd/8.3°Cd for R410A. In the end, condenser outlet temperatures were very similar for all refrigerants as ambient temperature was varied; see Figure 12. The effective temperature glides (thermodynamic + pressure drop) combined with the slightly different subcoolings resulted in similar, but slightly different dew point temperatures entering the condenser as shown in Figure 11. For example, at T_{amb} of 95°F/35°C, the entering dew point temperature with DR-55 is ~1°Fd/0.6°Cd higher than with R410A. In a simple thermodynamic cycle model, this increased lift costs about 1% in efficiency, offsetting some of the gain obtained from the higher evaporator exit dew point with DR-55 relative to R410A. When the evaporator and condenser effects are combined, the impact on efficiency matches the 4.3% advantage in efficiency observed in the tests (Schultz and Kujak, 2016).

9. CONCLUSIONS

Tests have been run with DR-55, DR-5A, and R32 in a rooftop heat pump unit as candidates for replacing R410A. Previous reports of overall performance showed DR-55 and DR-5A to be design-compatible with existing R410A-based equipment. This is further confirmed by the component level data presented here. The scroll compressor volumetric and isentropic efficiencies were observed to be essentially the same as R410A for DR-55 and DR-5A. When using R32, the volumetric efficiency dropped slightly (0.02 to 0.04) compared to R410A. R32's isentropic efficiency degraded relative to the others at ambient temperatures above 95°F/35°C.

The lower refrigerant flow rates that occurred with the alternatives relative to R410A (because of their wider domes) resulted in lower pressure drops and lower effective temperature glides. In particular, the inherent thermodynamic temperature glides of DR-55 and DR-5A nearly offset the negative temperature glides caused by pressure drop in the evaporator. This allowed DR-55 and DR-5A to operate with higher exiting dew points, reducing the effective temperature lift and thereby enhancing the efficiencies of these fluids relative to R410A. This also resulted in higher suction vapor densities, offsetting the thermodynamic shortfall in capacities relative to R410A.

In the condenser, the inherent thermodynamic temperature glide and pressure drop glide are additive. The impacts of DR-55's and DR-5A's higher thermodynamic glide are mitigated somewhat by the condenser's lower pressure drop characteristics combined with the lower flow rates. The refrigerant charge selection method (best efficiency) resulted in slightly different condenser exit subcooling for each refrigerant. The end result was very similar condenser exit temperatures (essentially the same approach temperatures) and slightly elevated entering dew point temperatures. The additional lift experienced with DR-55 and DR-5A offset a small portion of the efficiency gained from the higher evaporator exit dew points.

NOMENCLATURE

A_i	adjustment parameter for refrigerant *i*
COP	coefficient of performance (non-dim)
EER	energy efficiency ratio [Btu/W·hr]
GWP_{AR4}	Global Warming Potential in IPCC (2007)
GWP_{AR5}	Global Warming Potential in IPCC (2013)
h	enthalpy
$\dot{m}_{refrig}$	mass flow rate of refrigerant
P	pressure
Q_{air}	gross heat transfer rate from the indoor air stream as determined from measuring stations upstream and downstream of the indoor coil
$Q_{r,evap}$	heat transfer rate to the refrigerant flow through the indoor (evaporator) coil

S_{cmpr}	rotational speed of the compressor
s	entropy
SCOPc	seasonal average COP in cooling mode
SEER	seasonal energy efficiency ratio [Btu/W·hr]
T	temperature
T_{air}	weighted average of the indoor return air (65%) and delivered air (35%)
V_{cmpr}	volumetric displacement of the compressor
$\dot{V}_r$	volume flow rate of refrigerant
$\dot{W}_{cmpr}$	power input to compressor
η_{isen}	compressor isentropic efficiency
η_{vol}	compressor volumetric efficiency
ρ	density
υ	specific volume

Subscript

amb	ambient or outdoor condition
bbl	bubble point
cond	condenser
dew	dew point
dis	compressor discharge
evap	evaporator
in	inlet or entrance
meter	flow meter
out	outlet or exit
suc	compressor suction

REFERENCES

AHRI. 2016. AHRI Low-GWP Alternative Refrigerants Evaluation Program. See http://ahrinet.org/site/514/Resources/Research/AHRI-Low-GWP-Alternative-Refrigerants-Evaluation.

AHRI-210/240. 2008/2012. ANSI/AHRI Standard 210/240 with Addenda 1 and 2, 2008, Standard for Performance Rating of Unitary Air-Conditioning & Air-Source Heat Pump Equipment, AHRI, Arlington VA USA.

Hughes J, Leck T. 2015. Novel Reduced GWP Refrigerant Compositions for Stationary Air Conditioning. *Proceedings of the 24th IIR International Congress of Refrigeration: Yokohama, Japan, August 16-22*.

IPCC. 2007. *Climate Change 2007: The Physical Science Basis*. Contribution of Working Group I to the Fourth Assessment Report of the Intergovernmental Panel on Climate Change. Cambridge University Press, Cambridge, United Kingdom and New York, NY, USA.

IPCC. 2013. *Climate Change 2013: The Physical Science Basis*. Contribution of Working Group I to the Fifth Assessment Report of the Intergovernmental Panel on Climate Change. Cambridge University Press, Cambridge, United Kingdom and New York, NY, USA.

Kujak S, Schultz K. 2015. Performance Comparison of Optimized R410A Replacements. *Proceedings of the 24th IIR International Congress of Refrigeration: Yokohama, Japan, August 16-22*.

Kujak S, Schultz K. 2016. Optimizing the Flammability and Performance of Next Generation Low GWP R410A Replacements. Presented at the *ASHRAE Winter Conference, 24-27 Jan 2016, Orlando*, Conference Paper OR-16-C015. http://www.techstreet.com/ashrae/products/1874555.

Lemmon EW, Huber ML, McLinden, MO. 2013. NIST Standard Reference Database 23: Reference Fluid Thermodynamic and Transport Properties-REFPROP, Version 9.1, National Institute of Standards and Technology, Standard Reference Data Program, Gaithersburg, 2013.

Minor B. 2012. Intercompany communication.

Schultz K, Kujak S. 2016. Performance of 4-RT RTU with R410A Low GWP Alternatives. Presented at the *ASHRAE Annual Conference, 26-29 Jun 2016, St. Louis*, Conference Paper ST-16-C065.

Schultz K, Perez-Blanco M, Kujak S. 2015a. Soft-Optimized System Test of R410A, DR-55, R32, and DR-5A in a 4-Ton Unitary Rooftop Heat Pump, Cooling Mode Performance, Test Report #56 of the AHRI Low GWP AREP. The report is accessible from the AHRI 2016 link above.

Schultz K, Perez-Blanco M, Kujak S. 2015b. Soft-Optimized System Test of R410A, DR-55, R32, and DR-5A in a 4-Ton Unitary Rooftop Heat Pump, Heating Mode Performance, Test Report #57 of the AHRI Low GWP AREP. The report is accessible from the AHRI 2016 link above.